Supplementary Information

Indium oxide with oxygen vacancies boosts O_2 adsorption and activation for electrocatalytic H_2O_2 production

Danni Deng, Yuchao Wang, Jiabi Jiang, Yu Bai, Yingbi Chen,

Haitao Zheng, Houzheng Ou and Yongpeng Lei *

State Key Laboratory of Powder Metallurgy, Central South University,

Changsha 410083, China.

Correspondence and requests for materials should be addressed to Y. Lei.

（lypkd@163.com）

Experimental Section: S1-S5

Figures: S6-S21

Table: S22

Experimental Section

Materials

Indium nitrate hydrate (InN_3O_9) was directly obtained from Macklin Inc Co., Ltd. Urea ($CO(NH_2)_2$), potassium hydroxide (KOH) and commercial In_2O_3 were purchased from Sinopharm Chemical Reagent Co., Ltd. All aqueous solutions were prepared using deionized water obtained from Milli-Q ultrapure water (Millipore, ≥18.2 MΩ cm^{-1}). All of the reagents were of analytical grade (AR), and used without further purification.

Synthesis of In_2O_{3-x}

For In_2O_{3-x} synthesis, 0.38 g InN_3O_9 and 3 g urea were added to 20 mL H_2O, and sonicated for 30 min to ensure full dissolution. Then, the above solution was transferred into 50 mL Teflon-lined stain-less steel autoclave, heated at 120 ℃ for 12 h. After cooling down to room temperature, the suspension was collected and washed with H_2O/ethanol for several time. The white solid was dried overnight under vacuum at 60 °C and then underwent calcination in a muffle furnace at 600 °C (with a ramping rate of 5 °C min^{-1}) for 2 h to produce a yellow powder. Similar synthesis process was conducted to synthesize In_2O_{3-x}-400 and In_2O_{3-x}-800 with calcination temperature of 400 °C and 800 °C.

Synthesis of $In(OH)_3$

$In(OH)_3$ was prepared with the same process as that of In_2O_{3-x} except that the sample was not annealed.

Material characterizations

Scanning electron microscopy (SEM) was performed on a field emission scanning electron microscope (FEI Nova NanoSEM); energy-dispersive X-ray spectroscopy (EDS) and element mapping were conducted on SEM (Oxford X-MAX N 150 10 KV); The spherical aberration corrected transmission electron microscope (AC-TEM) was carried out on Thermo Fisher Spectra 300 (300 KV); X-ray diffractions were performed on X-ray diffractometer with Cu-Kα radiation (XRD, RIGAKU smart lab 1.6 KW, 40 KV, 40 mA, 1.5406 Å); X-ray photoelectron spectroscopy (XPS) was collected on an

Axia Ultra (Thermo Scientific ESCALab 250Xi+) XPS spectrometer equipped with an Al Kα source (1486.6 eV); The electron paramagnetic resonance (EPR) spectra were conducted on Bruker EMX PLUS (Center Field: 3510.00 G; Sweep Width: 100 G; Power: 10.8 mW; Frequency Mon: 9.853 GHz; Sweep Time: 19.456 s; Mod Amp: 1 G;). In-situ Raman spectra were conducted on a RTS2-301-SMS laser confocal Raman spectrometer equipped with 532 nm laser wavenumber as an excitation source. temperature programmed O_2 desorption (TPD-O_2) was performed on a TP-5080D adsorption instrument. The Zeta potential was carried out on a Malvern Zetasizer Nano ZS90 Zeta potential analyzer.

In-situ Raman spectroscopy

In-situ Raman spectra were collected at controlled electrochemical potentials in an electrochemical cell (3H gas diffusion type). The catalyst loaded on carbon paper (with a loading amount of 1.5 mg cm^{-2}) was used as the working electrode. Carbon rod and Ag/AgCl electrode were used as the counter and reference electrode, respectively. 1 M KOH saturated with oxygen bubbles was used as the electrolyte. Raman spectra were collected on a laser confocal Raman spectrometer (RTS2-301-SMS) excited by a 532 nm laser wavenumber with a power of 10 mW. And the flow rates of electrolyte and oxygen gas feed were set at 20 mL min^{-1} and 6 mL min^{-1}, respectively.

Electrochemical measurements

The ORR performances were evaluated with a three-electrode cell equipped with a rotating ring-disk electrode (RRDE) (Pine Research Instrumentation, USA) and CHI730E electrochemical workstation (Chenhua, Shanghai). Carbon rod was used as counter electrode, a saturated calomel electrode (SCE) was used as reference electrode, and the working electrode was RRDE loaded with catalyst. For preparing the working electrode, the catalyst ink was prepared by dispersing 6.0 mg of catalyst into 960 μL water-isopropanol solution (volume ratio of 3:1) and 40 μL Nafion (5 wt%) solution and sonicating for 30 min. After polishing RRDE mechanically with alumina suspension, 10 μL of catalyst ink was drop-casted onto the disk electrode (0.247 cm^2 area) of RRDE, resulting a catalyst loading of 24.2 μg cm^{-2} and then the electrode was

dried under an infrared lamp to give a uniform catalyst layer. Prior to the ORR measurement, the 0.1 M KOH electrolyte was saturated with O_2 for 30 min and kept saturated with O_2 during all the testing processes. Cyclic voltammetry (CV) scans at a rate of 100 mV s^{-1} from 1.2 V to 0 V vs. RHE were performed until a stable state was reached. Then, the LSV polarization curves were scanned from 1.0 V to 0 V vs. RHE at a rate of 5 mV s^{-1} with the RRDE rotating at 1600 rpm. The Pt ring electrode was held at 1.3 V vs. RHE to quantify the amounts of H_2O_2 produced on the disk electrode. The collection efficiency (N) on the RRDE electrode was calibrated in 0.1 M KCl + 10 mM $K_3Fe(CN)_6$ electrolyte at different rotation rates. Thus, the measured collection efficiency was determined to be 36%, which is reasonably close to the theoretical value. The H_2O_2 selectivity was calculated using the following equation:

$$H_2O_2\ (\%) = 200 \times \frac{\frac{I_r}{N}}{I_d + \frac{I_r}{N}}$$

Where I_r is the ring current, I_d is the disk current and N is the collection efficiency. The number of electrons transferred (n) was calculated using the equation:

$$n = 4 \times \frac{I_d}{I_d + \frac{I_r}{N}}$$

Electrochemical active surface area (ECSA) was conducted from double-layer charging curves using the CVs at the non-Faradic potential window in 0.1 M KOH. These samples were tested with scan rates ranging from 10 to 100 mV s^{-1}. The plots of current density (at 1.05 V vs. RHE) as a function of the scan rate showed the double-layer capacitance (C_{dl}) by the slopes.

Chronoamperometry stability test was conducted under a constant disk electrode potential at 0.5 V vs. RHE in O_2-saturated 0.1 M KOH electrolyte with the RRDE rotating speed of 1600 rpm. The Pt ring electrode was cleaned by CV scanning from 0 V to 1.2 V vs. RHE for 40 cycles.

All recorded potentials were calibrated to the reversible hydrogen electrode (RHE) using the equation $E_{RHE} = E_{SCE} + 0.0591*pH$.

Electrochemical measurements in Flow Cell

The electroreduction was further carried out in a gas diffusion electrode consisting of a coated In_2O_{3-x} catalyst as the working electrode, an anion exchange membrane, and commercial Nickel foams as the anode. Working electrode was prepared by spraying the catalyst onto a gas diffusion layer. Catalyst ink was prepared by mixing 20 mg catalyst, 100 μL 5 wt % Nafion solution and 2 mL ethanol. The ink was ultrasonically treated for 30 minutes before spraying, then sprayed on a gas diffusion (The loading capacity was controlled by 1 mg cm^{-2}.). The working electrode, an anion exchange membrane, and an anode of Nickel foams were then held together with a Polytetrafluoroethylene gasket. The liquid electrolyte can be introduced into a chamber between the anode and the membrane and between the membrane and the cathode. Gaseous O_2 diffuses from behind the gas diffusion layer to the liquid electrolyte in the catalytic region (1 × 2 cm^2). All the electrochemical experiments were tested at the CHI630 electrochemical workstation (Chenhua, Shanghai). The electrolyte (1 M KOH, 50 mL electrolytes for cathode and anode, respectively) was circulated in the electrochemical cell using a peristaltic pump.

H_2O_2 concentration quantification

A cerium sulfate ($Ce(SO_4)_2$) was used as an indicator to measure H_2O_2 concentration quantitatively. The quantification method is based on the color change from a yellow Ce^{4+} solution to a colourless Ce^{3+} by adding H_2O_2 as the reductant: $2Ce^{4+} + H_2O_2 \rightarrow 2Ce^{3+} + 2H^+ + O_2$. The concentration of Ce^{4+} before and after the reaction can be measured by ultraviolet-visible spectroscopy. Standard $Ce(SO_4)_2$ solution (0.5 mM) was prepared by dissolving $Ce(SO_4)_2$ salts into 0.5 M H_2SO_4. The calibration curves between absorbance and Ce^{4+} concentration were determined by measuring the absorbance at 318 nm of different $Ce(SO_4)_2$ solutions with known concentrations (0.01-0.05 mM). After electrolysis for a certain time period, 20 μL of the electrolyte in the cathode chamber after neutralization by 0.5 M sulfuric acid solution was added into the standard $Ce(SO_4)_2$ titrant solution. Based on the linear relationship between the signal intensity and Ce^{4+} concentration, the molar amounts of consumed Ce^{4+} after reaction

could be obtained. By this approach, the amounts of H_2O_2 produced can be calculated as half the molar amounts of the Ce^{4+} consumed ($2*C_{react(H2O2)} = C_{react(Ce4+)}$).The H_2O_2 productivity (mmol $g^{-1}_{catalyst}$ h^{-1}) and Faradaic efficiency (FE) were calculated as follows.

$$C_{H_2O_2}\,(mM) = \frac{V_{Ce^{4+}} \times C_{before_{Ce^{4+}}} - (V_{Ce^{4+}} + V_{removed\ electrolyte}) \times C_{after_{Ce^{4+}}}}{2 \times V_{removed\ electrolyte}}$$

$$H_2O_2\ productivity\ (mmol\ g^{-1}_{catalyst}\ h^{-1}) = \frac{C_{H_2O_2} \times V_{electrolyte}}{t \times g_{catalyst}}$$

$$FE\ (\%) = \frac{C_{H_2O_2} \times V_{electrolyte} \times 2 \times 96485}{Q}$$

Where $C_{H_2O_2}$ is the molarity of generated H_2O_2, $C_{before_{Ce4+}}$ is the molarity of the Ce^{4+} standard solution before the test, $C_{after_{Ce4+}}$ is the molarity of the Ce^{4+} solution after the test, V_{Ce4+} is the volume of the Ce^{4+} standard solution, $V_{removed\ electrolyte}$ is the volume of H_2O_2 solution removed from the electrolyte, and t is the electrolysis duration. $V_{electrolyte}$ is the catholyte volume. $g_{catalyst}$ is the mass of the catalyst. Q is the total amount of charge transferred.

Figures

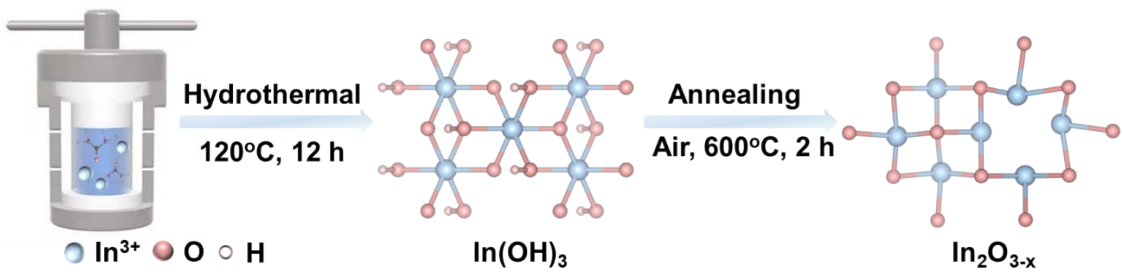

Figure S1. The schematic diagram of the synthesis of In_2O_{3-x}.

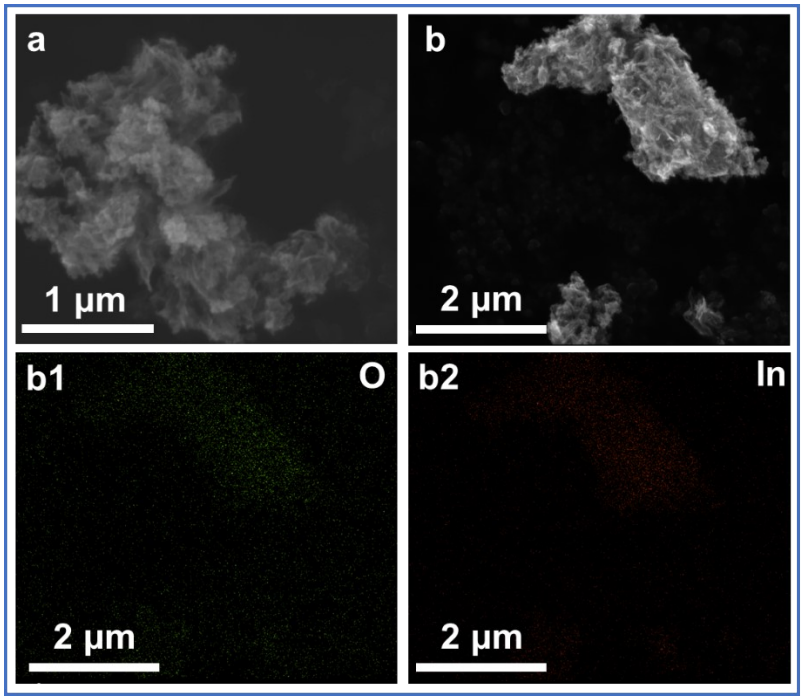

Figure S2. (a) SEM image and (b) SEM-EDS elemental mappings of In_2O_{3-x}.

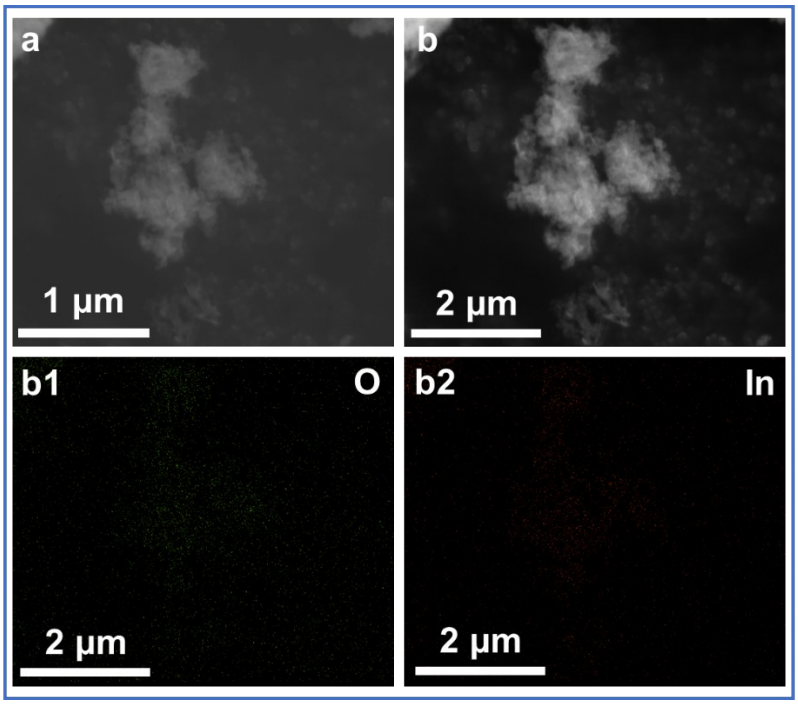

Figure S3. (a) SEM image and (b) SEM-EDS elemental mappings of $In(OH)_3$.

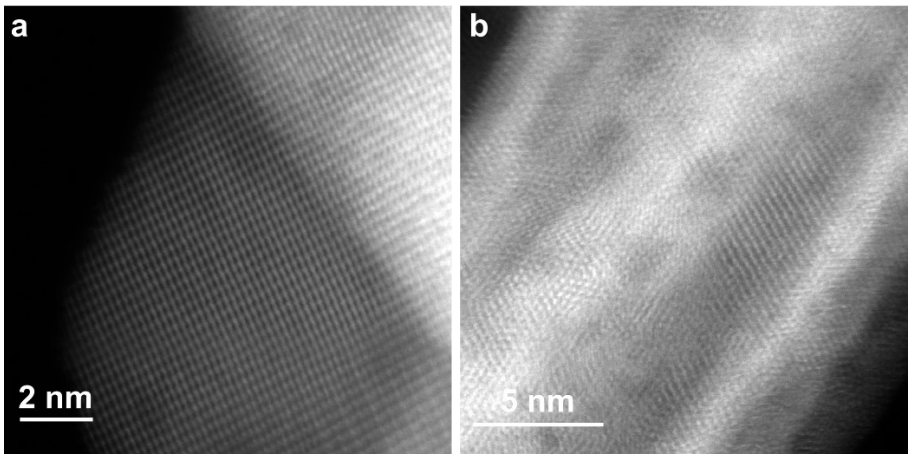

Figure S4. AC-TEM images (a) In_2O_{3-x} and (b) $In(OH)_3$.

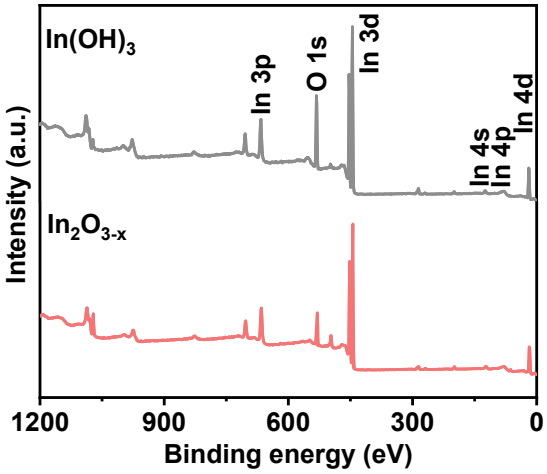

Figure S5. XPS survey spectra of In_2O_{3-x} and $In(OH)_3$.

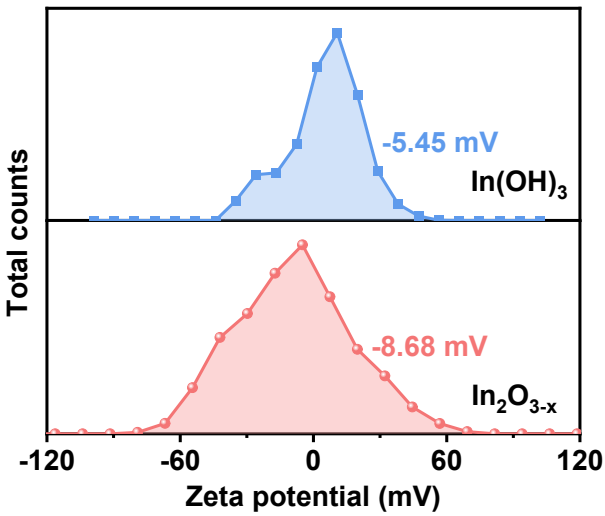

Figure S6. Zeta potential of In_2O_{3-x} and $In(OH)_3$.

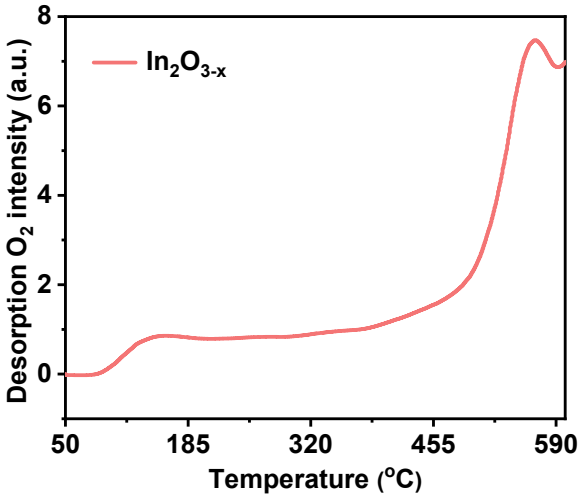

Figure S7. TPD-O_2 profile of In_2O_{3-x}.

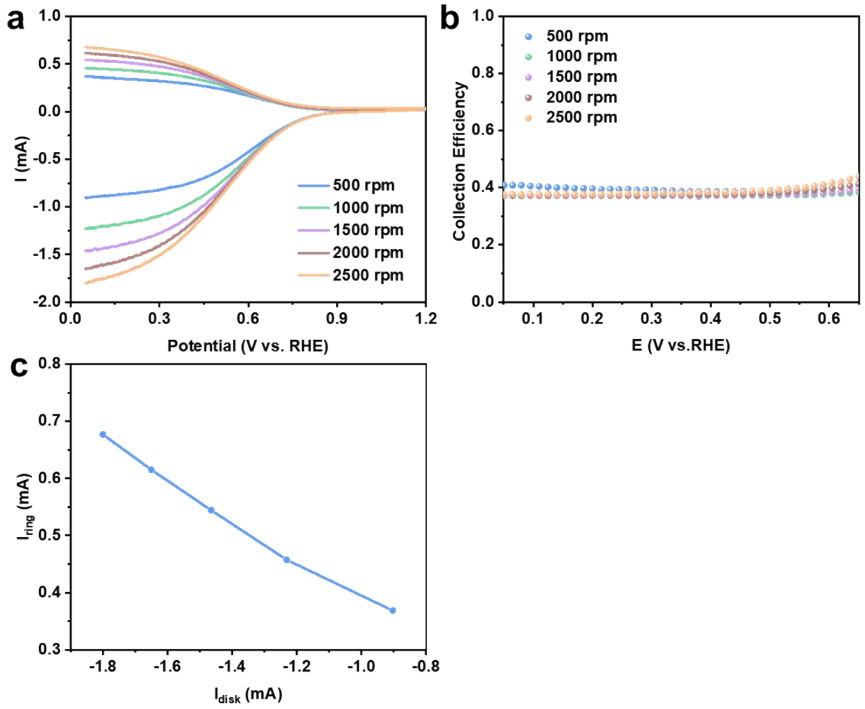

Figure S8. (a) RRDE voltammograms of glassy carbon electrode in 10 mM $K_3Fe(CN)_6$ and 0.1 M KCl with the disk and ring currents at 500, 1000, 1500, 2000 and 2500 rpm. The scan rate is 5 mV s^{-1} (1.3 V vs. RHE for ring). The calculated value of the collection efficiency at 1600 rpm is 0.36. (b) The corresponding collection efficiency of RRDE voltammograms as a function of the potential. (c) Linear fitting of the diffusion limited current recorded on disk and ring electrodes at different rotation speed.

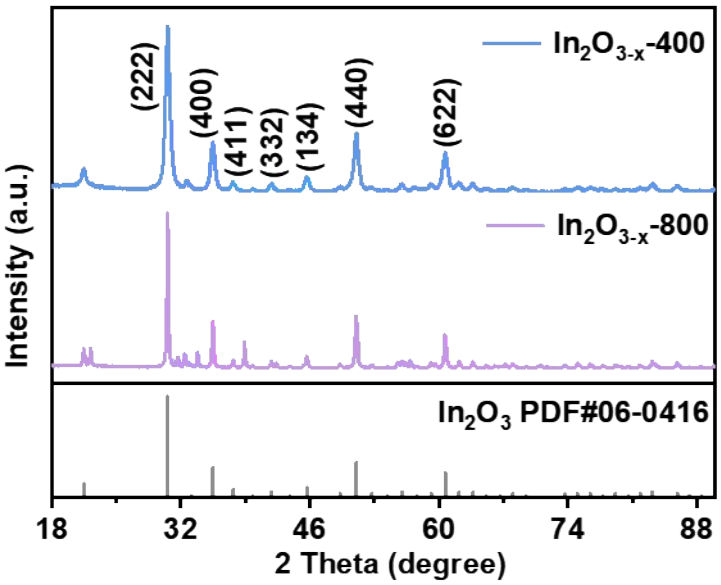

Figure S9. XRD patterns of In_2O_{3-x} annealed at 400 ℃ and 800 ℃.

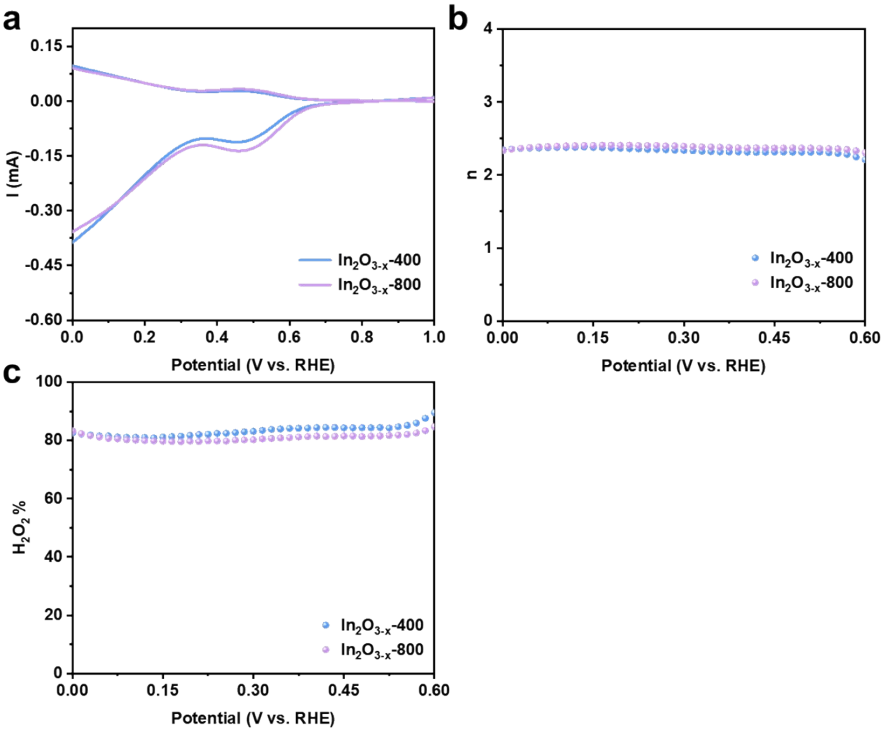

Figure S10. (a) LSV curves of In_2O_{3-x} annealed at 400 ℃ and 800 ℃. (b) The calculated n and (c) H_2O_2 selectivity of different samples.

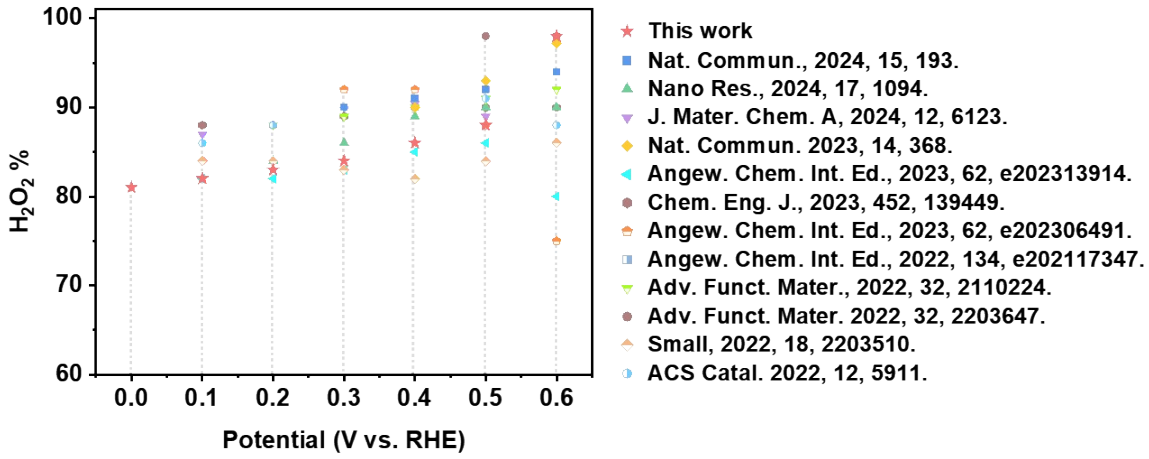

Figure S11. The H_2O_2 selectivity at different potential of In_2O_{3-x} and other reported catalysts based on RRDE performance.

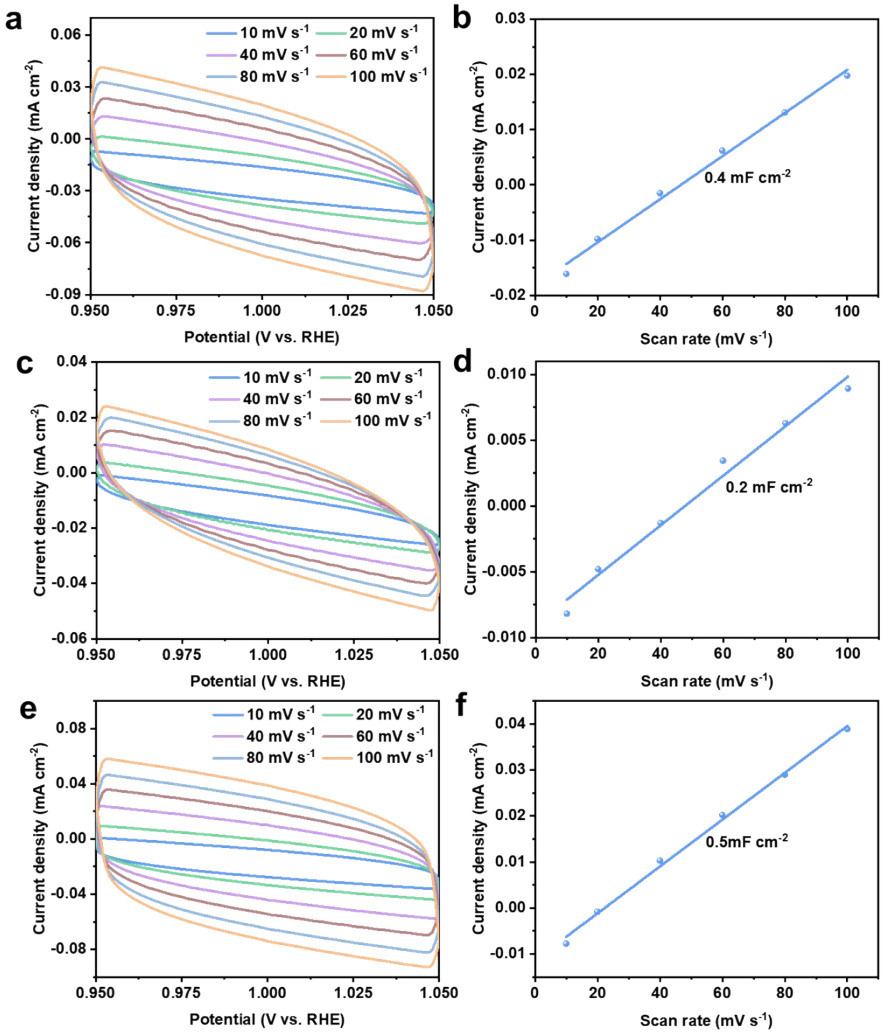

Figure S12. CV curves of (a) $In(OH)_3$, (c) commercial In_2O_3 and (e) In_2O_{3-x} in non-Faradaic potential region at different sweep rates ranging. Linear fitting of capacitive currents of (b) $In(OH)_3$, (d) commercial In_2O_3 and (f) In_2O_{3-x} vs. scan rate.

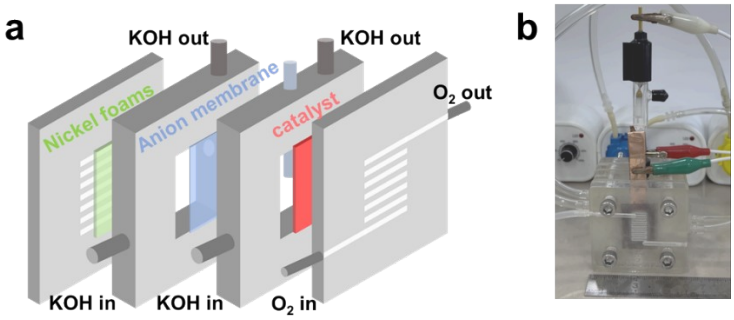

Figure S13. (a) The schematic diagram and (b) optical photograph of the flow cell.

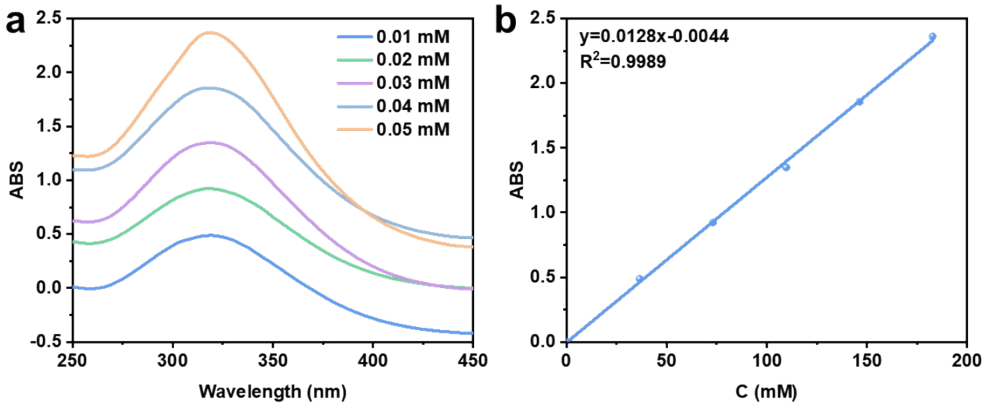

Figure S14. The concentrations of H_2O_2 in electrolytes were measured via the titration method using the standard ceric sulfate solutions, $Ce(SO_4)_2$: (a) UV-visible spectra of cerium titration and (b) the absorbance standard curves of different concentrations (0.01-0.05 mM) of $Ce(SO_4)_2$ solution.

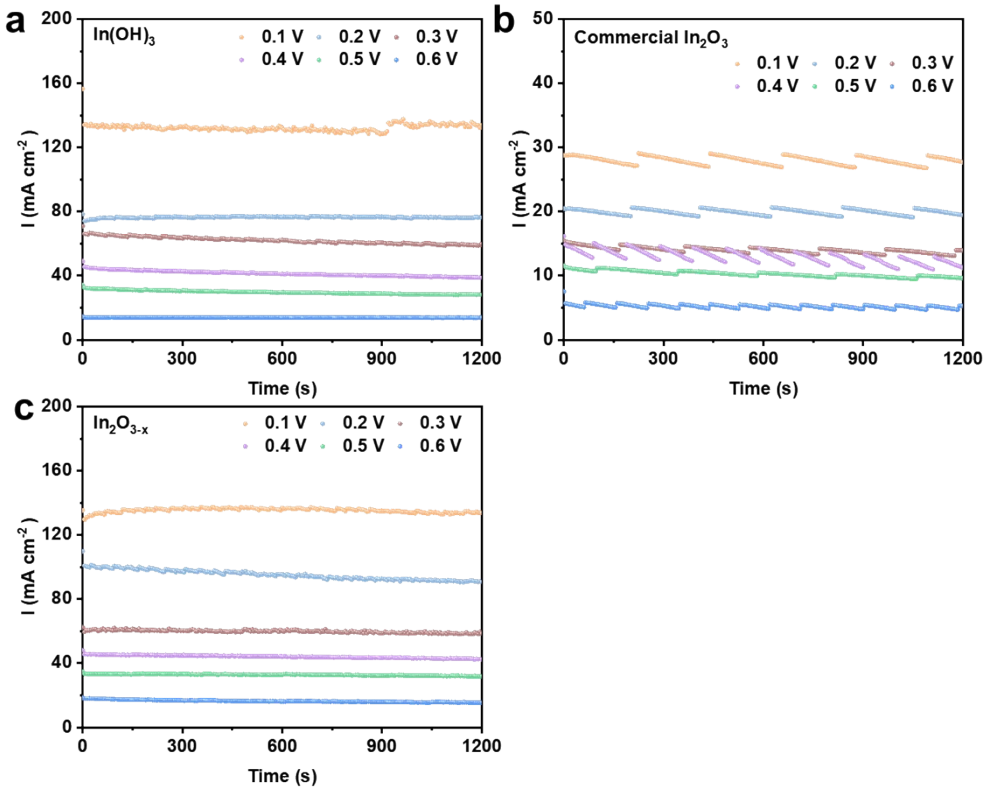

Figure S15. The chronoamperometry curves by flow cell test of (a) $In(OH)_3$, (b) commercial In_2O_3 and (c) In_2O_{3-x} in 1 M KOH.

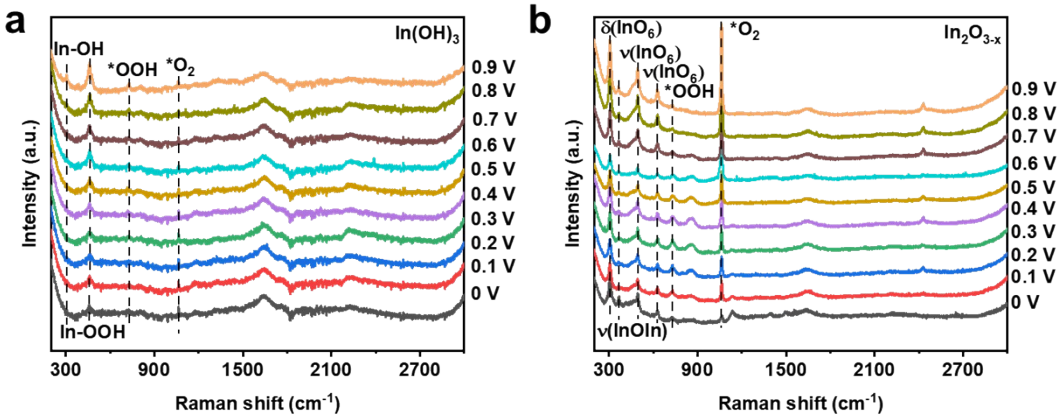

Figure S16. The in-situ Raman spectra of $In(OH)_3$ and In_2O_{3-x}.

Table

Table S1. $2e^-$ ORR performance of the various electrocatalysts in 0.1 M KOH.

Catalysts	Potential (V)	H_2O_2 Selectivity (%)	References
In_2O_{3-x}	0-0.6	81-98	This work
Pb SA/OSC	0.3-0.7	89-94	Nat. Commun., 2024, 15, 193.
Ni/CNS	0.2-0.7	84-90	Nano Res., 2024, 17, 1094.
ZnO	0.1-0.5	87-90.4	J. Mater. Chem. A, 2024, 12, 6123.
Sb-NSCF	0.4-0.7	90-97.2	Nat. Commun., 2023, 14, 368.
Zn-N_2O_2-S SAC	0.1-0.65	82-96	Angew. Chem. Int. Ed., 2023, 62, e202313914.
c-WO_3	0.1-0.6	88-90	Chem. Eng. J., 2023, 452, 139449.
FeSA-NS/C-700	0.3-0.5	92-75	Angew. Chem. Int. Ed., 2023, 62, e202306491.
In SAs/NSBC	0.4-0.7	93-95	Angew. Chem. Int. Ed., 2022, 134, e202117347.
W_1/NO-C	0.2-0.7	88-98	Adv. Funct. Mater., 2022, 32, 2110224.
In_2O_3/CDs-10	0.4-0.7	90-100	Adv. Funct. Mater., 2022, 32, 2203647.
Ni-B@BNC	0.2-0.6	84-92	Small, 2022, 18, 2203510.
NiOx-C	0.15-0.6	86-76	ACS Catal., 2022, 12, 5911.